Research Journal of Applied Sciences, Engineering and Technology 12(12): 1163-1175, 2016
DOI:10.19026/rjaset.12.2873
ISSN: 2040-7459; e-ISSN: 2040-7467

Submitted: April 22, 2014 Accepted: August 22, 2015 Published: June 15, 2016

**Research Article**

# Analysis of Finite Width Effects of Single-sided Linear Induction Motor Using Hankel Functions

Adhir Baran Chattopadhyay, Upala Banarjee and Sunil Thomas
Department of Electrical and Electronics Engineering, Birla Institute of Technology and Science,
P.O. Box: 345055, Pilani-Dubai, U.A.E

**Abstract:** Construction of a prototype Single Sided Linear Induction Motor (SLIM) is not possible taking stator and rotor width to be infinite because the formation of stator winding is not possible without the overhang. Also the current path in the rotor sheet cannot be made of closed type until and unless rotor width is finite. This study takes into account, the finite width effects of both stator and rotor but ignores the discontinuity of the rotor in the longitudinal direction. The finite width effects in a SLIM are analyzed using special mathematical tools such as Hankel Function for faster numerical convergence. The basic difficulty in formulating such problem, based on electromagnetic field theory applications, is to calculate the induced current in the rotor sheet, which is electrically decoupled from the stator winding system. It is also known that currents in the rotor sheet are generally computed, based on the fact that current cannot escape the sheet. Therefore, the divergence of rotor current density being zero calls for introduction of a field quantity "Stream Function". The present paper uses stream function effectively for tackling the above said difficulty. The results presented in the study are compared with the values of a model with stator and rotor of finite width. Such comparison results can help a designer to decide a finalized value of stator and rotor width.

**Keywords:** Hankel function, SLIM, stream function and finite width effects

## INTRODUCTION

Single Sided Linear Induction Motor (SLIM) is widely used in transportation system and other fields in need of linear drive which can obtain the thrust without gears and links, or auxiliary mechanisms. Bulk of literature deals with the double-sided, short primary and long secondary Linear Induction Motor (LIM) which is considered as one of the most suitable means of propulsion for high speed ground vehicles (Laithwaite, 1966). However, vehicles provided with these LIM's cannot provide good lift force because the strong attraction forces between primary and secondary iron dominates over the repulsive forces between primary winding and secondary conducting sheet (Nasar, 1976). Good amount of lift and propulsion can be obtained by using SLIM with long primary and short secondary (Chattopadhyay, 1997; Venkataratnam and Chattopadhyay, 2002). SLIM with short primary and long secondary consisting of a conducting plate lying on solid or laminated back iron has been analysed by many (Boldea and Babescu, 1978; Freeman and Lowther, 1973; Lipkins and Wang, 1971; McLean, 1988). But because of the discontinuity of the magnetic field in SLIM, they have special characteristics and inherent problems. Edge effect is one of the major phenomenons that makes the analysis and design of these motors difficult (Ham *et al*., 2009). Finite Width Effects have been analyzed by Preston and Reece (1969) the work presented in Han *et al*. (2008) is a field theory approach because original formulations have been done in terms of vector potential. However dynamic characteristics have not been dealt in detail. Analysis presented in Yang *et al*. (2008) appears to be more helpful for a designer as it is based on circuit theory approach. It is well known that numerical methods in computational techniques becomes very much helpful to a researcher or designer when the electromagnetic field equations are applied to a full electrical machine or parts of electrical machines in the proximity of iron boundary. Such philosophy leads to partial differential equations or integro-differential equations formulation in the area of electrical machines, drives or magnetic. As realistic iron boundaries are involved in such formulations, closed form equations becomes very difficult to build up and hence the concerned analytical solutions are also rare. Such situations can be tackled efficiently using tools under numerical methods such as finite difference method, finite element method etc. In such context the companion paper (Dos Santos *et al*., 2001) draws the attention of researchers. In such paper the mathematical

**Corresponding Author:** Adhir Baran Chattopadhyay, Department of Electrical and Electronics Engineering, Birla Institute of Technology and Science, P.O. Box: 345055, Pilani-Dubai, Tel.: 00971-4-2700400

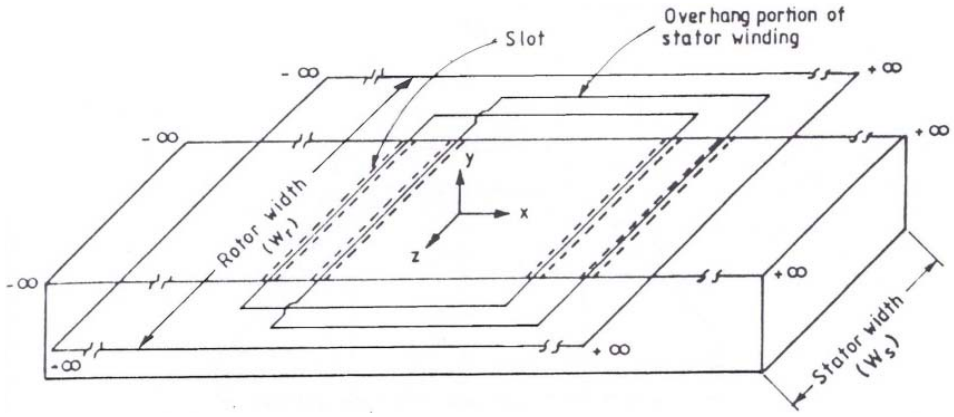


Fig. 1: Model of SLIM with coordinate system used for analysis of finite width effects (Coordinate axes are fixed relative to rotor)

model has been developed from the view point of circuit theory and hence equivalent circuit is feasible. But finite element method has been applied efficiently to the system to calculate the propelling force which is generally considered to be one of the major components of electromagnetic forces. The dynamic end effects of a Linear Induction Motor [LIM] are needed to be calculated with much accuracy for the betterment of the design process. The concept of state space vector model of a Lim can be applied to calculate the net axial thrust including the end effect braking force (Pucci, 2014). For practical application of a particular LIM as a component of machine drives needs for the clear cut declarations of the machine design parameters. Such parameters if needed are to be calculated becomes cumbersome job. Alternately parameter identification can be done based on input, output data. Exactly this type of work has been reported by Alonge *et al*. (2014). The present paper analyses the transverse edge effects in a SLIM using field theory approach. The results regarding the electromagnetic forces presented in this study can be compared to a realistic model with stator and rotor of finite width. In a practical machine the width of the stator winding as well as the width of the supporting back iron must be finite. The width of the rotor sheet placed over the stator winding of finite width can be made very large but it has no practical advantage beyond certain extent. From the experimental results, it is observed that the rotor width should be approximately equal to stator width including winding overhang for good performance. Therefore the rotor width is also finite. Length of the rotor sheet should also be finite because concept of infinite length is absurd. But to analyse the problem in stages, a rotor of infinite length and finite width is considered in the present paper. With reference to Fig. 1, we propose to calculate:

- The field at any point in free space due to the stator winding having a sinusoidal distribution of linear current density along the length
- The induced currents in the rotor sheet considering the field due to stator as well as the rotor currents
- The propulsion, levitation and lateral forces on the rotor

The coordinate system is fixed relative to the rotor, the origin being placed just above the stator surface. The rotor is assumed to be thin and lying parallel to x-z plane at a height h from the stator surface. It is also assumed that the stator back iron of width Ws, is assumed to be infinitely permeable and perfectly laminated.

## MATERIALS AND METHODS

**Formulation for the field due to stator current sheet:** As the stator winding has finite width, the stator current will have not only the axial component of the linear current density, $j_z$ (which would have been the only component for a stator winding of infinite width) but also the peripheral component of linear current density, $j_x$. The latter component may be viewed as one due to the end current of a winding having overhang. From the physical considerations, the axial component of linear current density can be assumed to be constant over the stator iron width. For diamond shaped coils, the variation of $j_z$ with the overhang width can be considered as linear. Therefore, in a coordinate system fixed to the rotor, $j_z$ (Ratnam and Chattopadhyay, 1996) can be expressed as:

$$j_z = I_z f(z) e^{j(s\omega_s t - kx)} \quad (1)$$

where,

$I_z$ = Peak value of stator linear current density
$\omega_s$ = Supply frequency in rad/sec

$$k = \pi/\tau$$

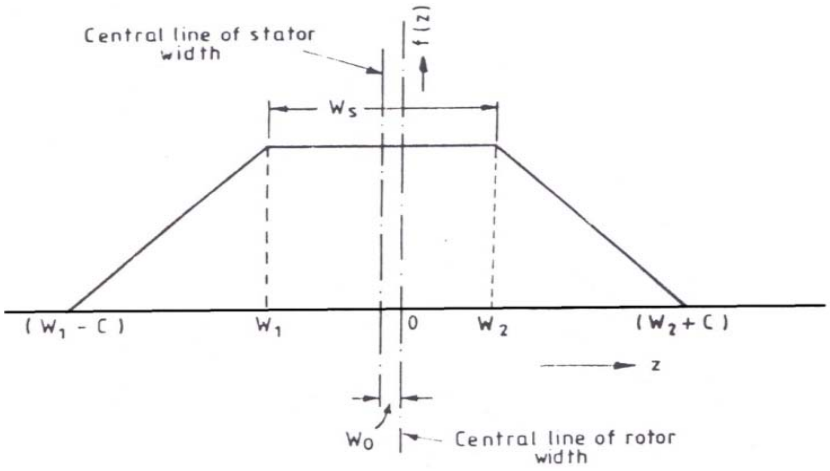


Fig. 2: Variation of f (z) with z

where,
$\tau$ = Stator pole-pitch
$s$ = Slip of the rotor

The function of f(z) in Eq. (1) can be expressed as given in Fig. 2:

$$f(z) = 1 \text{ for } W_1 < z < W_2 \quad (2)$$

$$= 1 - \frac{(z-W_2)}{C} \text{ for } W_2 < z < (W_2+C) \quad (3)$$

$$= 1 + \frac{(z-W_1)}{C} \text{ for } (W_1-C) < z < W_1 \quad (4)$$

where,
C = Stator overhang length (in z direction)

$$W_1 = -\frac{W_s}{2} - W_0 \quad (5)$$

$W_s$ = Width of the stator iron block
$W_0$ = Offset of the rotor sheet (widthwise) with respect to the stator:

$$W_2 = \frac{W_s}{2} - W_0 \quad (6)$$

It is necessary to assume certain amount of offset for the rotor (W0) with respect to the stator to enable calculation of the lateral force. The continuity equation of the current in the stator winding can be expressed as:

$$\frac{dj_z}{dz} + \frac{dj_x}{dx} = 0 \quad (7)$$

As an infinitely long three phase balanced distributed stator winding fed by three phase balanced currents can be represented by a current sheet having a sinusoidal current distribution along the length and with respect to time, like $j_z$ expressed in Eq. (1):

$j_x$ can also be expressed as $j_x = j_{x0}\, e^{j(s\omega_s t - Kx)}$ (8)

$j_{x0}$ = The function of z only.

From Eq. (1) and (8) we have:

$$\frac{dj_z}{dz} = I_z f'(z) e^{j(s\omega_s t - kx)} \quad (9)$$

$$\frac{dj_x}{dz} = (-jk) j_{x0} e^{j(s\omega_s t - kx)} \quad (10)$$

$f'(z)$ is the derivative of $f(z)$ with respect to z. Eq. (7) (9) and Eq. (10) yield:

$$j_{x0} = -j\left(\frac{I_z}{k}\right) f'(z) \quad (11)$$

From Eq. (8), (11) we can express:

$$j_x = -j\left(\frac{I_z}{k}\right) f'(z) e^{j(s\omega_s t - kx)} \quad (12)$$

**Vector potential due to stator current:** The vector potential due to stator current at any field point (x', y', z') can be expressed as:

$$\overrightarrow{A_{I1}} = \frac{\mu_0}{4\pi} \int_{W_1-C}^{W_2+C} \int_{-\infty}^{\infty} \frac{j_x \vec{i} + j_z \vec{k}}{r}\, dx\, dz \quad (13)$$

where

$$r = \sqrt{(x - x')^2 + (y')^2 + (z - z')^2} \quad (14)$$

Is the distance of the field point (x', y', z') from the source point (x, 0, z). The effect of stator iron is taken into account by considering the 'image' of $j_z$ over the width of the iron block, $W_s$, which will contribute an additional component vector potential given by:

$$\overrightarrow{A_{I2}} = \frac{\mu_0}{4\pi} \int_{W_1}^{W_2} \int_{-\infty}^{\infty} \frac{j_z \vec{k}}{r}\, dx\, dz \quad (15)$$

The image of $j_x$ is not taken into account as it flows in the overhang beyond stator iron width. Thus the vector potential at any field point:

$$\overrightarrow{A_I} = \overrightarrow{A_{I1}} + \overrightarrow{A_{I2}} \tag{16}$$

Based on Eq. (13) and (15), we have $\overrightarrow{A_{I1}}$ and $\overrightarrow{A_{I2}}$ :

$$\overrightarrow{A_{I1}} = \left[\frac{\mu_0}{4\pi}\left(-j\frac{I_z}{k}\right)e^{js\omega_s t}\left[\int_{W_1-C}^{W_2+C} f'(z)\left\{\int_{-\infty}^{\infty}\frac{e^{-jkx}}{r}\,dx\right\}dz\right]\right]\vec{\imath} + \left[\frac{\mu_0}{4\pi} I_z e^{js\omega_s t}\left[\int_{W_1-C}^{W_2+C} f(z)\left\{\int_{-\infty}^{\infty}\frac{e^{-jkx}}{r}\,dx\right\}dz\right]\right]\vec{k} \tag{17}$$

$$\overrightarrow{A_{I2}} = \left[\frac{\mu_0}{4\pi} I_z e^{js\omega_s t}\left[\int_{W_1}^{W_2} f(z)\left\{\int_{-\infty}^{\infty}\frac{e^{-jkx}}{r}\,dx\right\}dz\right]\right]\vec{k} \tag{18}$$

Eq. (17) and (18) involve an integral which can be rewritten using Eq. (14) as:

$$\int_{-\infty}^{\infty}\frac{e^{-jKx}}{r}\,dx = \int_{-\infty}^{\infty}\frac{e^{-jkx}}{\sqrt{(x-x')^2+(y')^2+(z-z')^2}}\,dx$$

On simplification by contour integration method (Details given in Appendix-1) we finally get:

$$\int_{-\infty}^{\infty}\frac{e^{-jKx}}{r}\,dx = 2e^{-jKx'}\int_1^{\infty}\frac{e^{-kbt_1}}{\sqrt{({t_1}^2-1)}}\,dt_1 \tag{19}$$

The integral on the R.H.S of Eq. (19) can be written as Preston and Reece (1969) and Pucci (2014):

$$2\int_1^{\infty}\frac{e^{-kbt_1}}{\sqrt{({t_1}^2-1)}}\,dt_1 = 2\pi j\,H_0^{(1)}$$

where, $H_0^{(1)}$ is the Hankel function of the zeroth order of the first kind. The numerical evaluation of this integral is much faster as compared to that of the original integral in the L.H.S of Eq. (19). Based on Eq. (16), (17), (18) and (19) the net vector potential $\overrightarrow{A_I}$, at any field point due to the stator current can be expressed as:

$$\overrightarrow{A_I} = \frac{\mu_0}{4\pi}\left(-j\frac{I_z}{k}\right)e^{js\omega_s t} e^{-jkx'}\left[\int_{W_1-C}^{W_2+C} 2f'(z)\left\{\int_1^{\infty}\frac{e^{-kbt_1}}{\sqrt{({t_1}^2-1)}}\,dt_1\right\}dz\right]\vec{\imath} + \frac{\mu_0}{4\pi} I_z e^{js\omega_s t}\, e^{-jkx'}\left[\left\{\int_{W_1-C}^{W_2+C} 2f(z)\left\{\int_1^{\infty}\frac{e^{-kbt_1}}{\sqrt{({t_1}^2-1)}}\,dt_1\right\}dz\right\} + \left\{\int_{W_1}^{W_2} 2f(z)\left\{\int_1^{\infty}\frac{e^{-kbt_1}}{\sqrt{({t_1}^2-1)}}\,dt_1\right\}dz\right\}\right]\vec{k} \tag{20}$$

The integration over 'z' can be carried out numerically without any further transformation because of the finite limits of 'z'.

From the vector potential $\overrightarrow{A_I}$ expressed in Eq. (20), the flux density vector at any field point can be computed numerically using the relation $\vec{B} = \nabla \times \vec{A}$. Numerical algorithms are presented in later sections.

**Formulation for current and fields in the rotor sheet:** With reference to Fig. 1, the rotor sheet is placed parallel to the surface of the stator with its longitudinal edges running parallel to the length of the stator. As the rotor sheet is of finite width like the stator, the induced currents in the sheet must have a closed path. Therefore the axial component of the rotor current density $(J_z)$ must gradually turn into peripheral current density $(J_x)$. The rotor sheet has small thickness and hence it does not allow any normal component of current density, $J_y$, to flow. In other words, the rotor current is planar in nature. At any instant, in the sheet, divergence of the current density must vanish to maintain continuity of current flow. Therefore we can write:

$$\vec{\nabla}.\vec{J} = 0 \tag{21}$$

As divergence of curl of any vector is zero, $\vec{J}$ can be expressed in terms of stream function $\vec{u}$ as:

$$\vec{J} = \vec{\nabla} \times \vec{u} \tag{22}$$

As planar current flows in the sheet, the stream function possesses only one component, $u_y$, normal to its surface:

$$\vec{\nabla} \times \vec{J} = \vec{\nabla}\left(\vec{\nabla}.\vec{u}\right) - \nabla^2\vec{u} \tag{23}$$

As $u_x = u_z = 0$ and $u_y$ does not vary with y, hence $\vec{\nabla}.\vec{u} = 0$:

$$\vec{\nabla} \times \vec{J} = 0\vec{\imath} + \left(-\nabla^2 u_y\right)\vec{J} + 0\vec{k} \tag{24}$$

$$\vec{J} = \sigma\vec{E} \text{ and } \vec{\nabla} \times \vec{E} = -\frac{\partial\vec{B}}{\partial t}$$

where $\vec{E}$ is the electric field vector and $\sigma$ is the conductivity of the rotor sheet material:

$$\vec{\nabla} \times \vec{J} = -\sigma\frac{\partial\vec{B}}{\partial t} = 0\vec{\imath} + \left(-\sigma\frac{\partial B_y}{\partial t}\right)\vec{J} + 0\vec{k} \tag{25}$$

where, $B_y$ is the total flux density (normal to the sheet) at the field point (x', y', z') on the sheet. As $'B_y'$ has a sinusoidal variation with respect to time, we can write:

$$\frac{\partial B_y}{\partial t} = js\omega_s B_y \quad (26)$$

Substituting Eq. (26) in Eq. (25), we obtain:

$$\vec{\nabla} \times \vec{J} = (-j\sigma s\omega_s B_y)\vec{j} \quad (27)$$

Equating R.H.S of Eq. (24) and (27), we obtain (Nasar, 1976):

$$\nabla^2 u_y = j\sigma s\omega_s B_y \quad (28)$$

$$\frac{\partial^2 u_y}{\partial x'^2} + \frac{\partial^2 u_y}{\partial z'^2} = j\sigma s\omega_s B_y \quad (29)$$

As the rotor sheet is of infinite length, like stator linear current density components, rotor linear current density components also will have sinusoidal variation in the longitudinal direction. Therefore at any point (x', y', z') in the sheet, $u_y$ is:

$$u_y = (u_y(z'))e^{-jkx'} \quad (30)$$

where, $u_y(z')$ is a function of $z'$ only. From Eq. (30) we obtain:

$$\frac{\partial^2 u_y}{\partial x'^2} = -k^2(u_y(z'))e^{-jkx'} \quad (31)$$

$$\frac{\partial^2 u_y}{\partial z'^2} = \frac{d^2(u_y(z'))}{dz'^2}e^{-jkx'} \quad (32)$$

Eq. (29), (31) and (32) yield:

$$\left[\frac{d^2(u_y(z'))}{dz'^2} - k^2(u_y(z'))\right]e^{-jkx'} = j\sigma s\omega_s B_y \quad (33)$$

Along with boundary condition $u_y\big|_{z'=-\frac{W_r}{2}} = 0$ and $u_y\big|_{z'=\frac{W_r}{2}} = 0$ (34)

where, $W_r$ is the width of the rotor sheet. The boundary conditions indicate that current cannot escape from the rotor sheet along its width. $'B_y'$ in Eq. (33) can be obtained as:

$$B_y = B_{y1} + B_{y2} \quad (35)$$

where, $B_{y1}$ is the normal component of the flux density due to the stator current sheet (obtained as explained at the end of above section) and $B_{y2}$ is the normal component of flux density due to the rotor current taking into account the proximity of stator iron. The formulation and calculation of $B_{y2}$ is presented in following section.

**Vector potential due to rotor current:** The vector potential, $\overrightarrow{A_2}$ at any field point (x', z') in the rotor sheet due to currents in the same sheet, taking into account the proximity of stator back iron is given by:

$$\overrightarrow{A_2}(x', z') = \overrightarrow{A_{21}} + \overrightarrow{A_{22}} \quad (36)$$

$$\overrightarrow{A_{21}} = \frac{\mu_0}{4\pi}\left[\int_{-\frac{W_r}{2}}^{\frac{W_r}{2}}\int_{-\infty}^{\infty}\frac{j_{xr}\,\vec{i} + j_{zr}\,\vec{k}}{r_1}\,dx\,dz\right] \quad (37)$$

$$\overrightarrow{A_{22}} = \frac{\mu_0}{4\pi}\left[\int_{W_1}^{W_2}\int_{-\infty}^{\infty}\frac{j_{xr}\,\vec{i} + j_{zr}\,\vec{k}}{r_2}\,dx\,dz\right] \quad (38)$$

where, $r_1 = \sqrt{(x - x')^2 + (z - z')^2}$ and $r_2 = \sqrt{(x - x')^2 + (z - z')^2 + 4(y')^2}$

where, $y'$ is the height of the rotor sheet above the stator surface. With reference to Eq. (37) and Eq. (38), $\overrightarrow{A_{21}}$ and $\overrightarrow{A_{22}}$ are the vector potentials due to rotor current and its image over the stator iron width respectively. $j_{xr}$ and $j_{zr}$ are the longitudinal and lateral components of the rotor sheet. Vector potential due to rotor currents has similar expressions as those due to stator current, except that the rotor current density components are unknown unlike the components in the stator winding. Hence:

$$j_{xr} = dJ_{xr}\ ;\ j_{zr} = dJ_{zr} \quad (39)$$

where, $J_{xr}, J_{zr}$ are the rotor current density components (in A/m$^2$) and $'d'$ is the thickness of the rotor sheet. From the relation $\vec{J} = \vec{\nabla} \times \vec{u}$ $J_{xr}$ and $J_{zr}$ can be expressed as:

$$J_{xr} = -\frac{\partial u_y}{\partial z}\ ;\ J_{zr} = \frac{\partial u_y}{\partial x} \quad (40)$$

From Eq. (39) and Eq. (40) we obtain:

$$j_{xr} = -d\frac{\partial u_y}{\partial z}\ ;\ j_{zr} = d\frac{\partial u_y}{\partial x} \quad (41)$$

From Eq. (30) we can write:

$$\frac{\partial u_y}{\partial z} = \frac{du_y}{dz}\,e^{-jkx}\ ;\ \frac{\partial u_y}{\partial x} = (-jk)u_y e^{-jkx} \quad (42)$$

$u_y$ Appearing on the R.H.S of Eq. (42) equations is a function of $'z'$ only. Based on Eq. (41) and Eq. (42) we can write:

$$j_{xr} = -d\frac{du_y}{dz}\,e^{-jkx}\ ;\ j_{zr} = d(-jk)u_y e^{-jkx} \quad (43)$$

Based on Eq. (36), (37), (38), (43), $\overrightarrow{A_2}(x', z')$ can be written as:

$$\overrightarrow{A_2} = \overrightarrow{A_{2x}}\,\vec{i} + \overrightarrow{A_{2z}}\,\vec{k} \quad (44)$$

$$A_{2x} = \frac{\mu_0 d}{4\pi}\left[\int_{-\frac{W_r}{2}}^{\frac{W_r}{2}}\left(-\frac{du_y}{dz}\right)\left\{\int_{-\infty}^{\infty}\frac{e^{-jkx}}{\sqrt{(x-x')^2+(z-z')^2}}\,dx\right\}dz\right] + \frac{\mu_0 d}{4\pi}\left[\int_{W_1}^{W_2}\left(-\frac{du_y}{dz}\right)\left\{\int_{-\infty}^{\infty}\frac{e^{-jkx}}{\sqrt{(x-x')^2+(z-z')^2+4(y')^2}}\,dx\right\}dz\right] \quad (45)$$

$$A_{2z} = \frac{\mu_0 d}{4\pi}\left[\int_{-\frac{W_r}{2}}^{\frac{W_r}{2}}(-jk)u_y\left\{\int_{-\infty}^{\infty}\frac{e^{-jkx}}{\sqrt{(x-x')^2+(z-z')^2}}\,dx\right\}dz\right] + \frac{\mu_0 d}{4\pi}\left[\int_{W_1}^{W_2}(-jk)u_y\left\{\int_{-\infty}^{\infty}\frac{e^{-jkx}}{\sqrt{(x-x')^2+(z-z')^2+4(y')^2}}\,dx\right\}dz\right] \quad (46)$$

The infinite limit integrals appearing in Eq. (45) and (46) can be reduced again by the method of contour integration, similar to the method followed in above section. (For details refer Appendix-1). Thus $\overrightarrow{A_{2x}}$ and $\overrightarrow{A_{2z}}$ can be simplified to the expressions given by:

$$A_{2x} = \frac{2\mu_0 d}{4\pi}e^{-jkx'}\left[\int_{-\frac{W_r}{2}}^{\frac{W_r}{2}} - \frac{du_y}{dz}\left\{\int_1^{\infty}\frac{e^{-kt_1(z-z')}}{\sqrt{({t_1}^2-1)}}\,dt_1\right\}dz\right] + \frac{2\mu_0 d}{4\pi}e^{-jkx'}\left[\int_{W_1}^{W_2} - \frac{du_y}{dz}\left\{\int_1^{\infty}\frac{e^{-kt_1\sqrt{(z-z')^2+4(y')^2}}}{\sqrt{({t_1}^2-1)}}\,dt_1\right\}dz\right] \quad (47)$$

$$A_{2z} = \frac{2\mu_0 d}{4\pi}e^{-jkx'}\left[\int_{-\frac{W_r}{2}}^{\frac{W_r}{2}}(-jk)u_y\left\{\int_1^{\infty}\frac{e^{-kt_1|z-z'|}}{\sqrt{({t_1}^2-1)}}\,dt_1\right\}dz\right] + \frac{2\mu_0 d}{4\pi}e^{-jkx'}\left[\int_{W_1}^{W_2}(-jk)u_y\left\{\int_1^{\infty}\frac{e^{-kt_1\sqrt{(z-z')^2+4(y')^2}}}{\sqrt{({t_1}^2-1)}}\,dt_1\right\}dz\right] \quad (48)$$

**Solution of stream function, $u_y$:** In Eq. (33), the normal component for flux density, $B_y$ comprises of $B_{y1}$, the component due to stator current and $B_{y2}$, the component due to rotor current. At any point on the rotor sheet, $B_{y1}$ can be calculated from the vector potential, $\overrightarrow{A_1}$ due to known stator current as given in Eq. (20). Similarly $B_{y2}$ can be obtained from $A_{2x}$ and $A_{2z}$ (Eq. (47) and (48)) which are integrals involving the unknown $u_y$ and its partial derivatives with appropriate kernels. Equation (20) has on its L.H.S the unknown function $u_y$ and its second order derivative while the R.H.S involves a known function, $B_{y1}$ and the integral expression involving $u_y$ and its partial derivatives with suitable kernels. Thus Eq. (20) is an integro-differential equation in $u_y$. It is perhaps possible to solve such equation analytically using some sort of integral transforms. However, the kernel involved in this equation is singular and difficult to handle mathematically. Hence numerical solution to the problem is preferred. Step by step method for solution of $u_y$ is outlined in next section.

Steps of algorithm for numerical solution for $u_y$ and $B_{y2}$:

**Step 1:** The rotor sheet is discretized along its width (in z-direction) into a large number of elements each of width 'dz'. Discretizing the rotor sheet along the length (in the x-direction is not necessary). The coordinates of the grid point along the width are noted.

**Step 2:** Calculation of flux density ($B_{y1}$) due to the stator current:

Rearranging the expression for the vector potential due to stator current sheet, $\overrightarrow{A_I}$ in Eq. (20), we obtain, for a fixed value of $y'$:

$$\overrightarrow{A_I} = \left[A_{1x}(z')\,\vec{\imath} + A_{1z}(z')\,\vec{k}\right]e^{-jkx'}e^{js\omega_s t} \quad (49)$$

where,

$$A_{1x}(z') = \frac{\mu_0}{4\pi}\left(-j\frac{I_z}{k}\right)\left[\int_{-\frac{W_r}{2}}^{\frac{W_r}{2}}2f'(z)\left\{\int_1^{\infty}\frac{e^{-kbt_1}}{\sqrt{({t_1}^2-1)}}\,dt_1\right\}dz\right] \quad (50)$$

$$A_{1z}(z') = \frac{\mu_0}{4\pi}I_z\left[\int_{-\frac{W_r}{2}}^{\frac{W_r}{2}}2f(z)\left\{\int_1^{\infty}\frac{e^{-kbt_1}}{\sqrt{({t_1}^2-1)}}\,dt_1\right\}dz + \int_{W_1}^{W_2}2f(z)\left\{\int_1^{\infty}\frac{e^{-kbt_1}}{\sqrt{({t_1}^2-1)}}\,dt_1\right\}dz\right] \quad (51)$$

The flux density at any point due to the stator current $B_{y1}$ can be expressed as:

$$B_{y1} = (B_{y1}(z'))e^{-jkx'} \quad (52)$$

where,

$$B_{y1}(z') = \frac{d\left(A_{1x}(z')\right)}{dz'} + jk\,A_{1z}(z') \quad (53)$$

The grid points obtained after discretizing the sheet are used to calculate $\overrightarrow{A_I}$ and then $B_{y1}(z')$ using Eq. (49) and (53). The required numerical differentiation has been carried out by forward difference method. Thus a column matrix $[B_{y1}]$ is formed.

**Step 3:** Calculations of normal component of flux density due to rotor current, $B_{y2}$.

The expression for the component of vector potential, $A_{2x}$ and $A_{2z}$, at any point in the sheet due to rotor current, can be rewritten, based on Eq. (47) and (48) respectively, as:

$$A_{2x|_{(x',y',z')}} = A_{2x}(z')\, e^{-jkx'} \tag{54}$$

$$A_{2z|_{(x',y',z')}} = A_{2z}(z')\, e^{-jkx'} \tag{55}$$

$$A_{2x}(z') = \frac{2\mu_0 d}{4\pi}\left[\int_{-\frac{W_r}{2}}^{\frac{W_r}{2}} -\frac{d(u_y(z))}{dz}\left\{\int_1^{\infty}\frac{e^{-kt_1(z-z')}}{\sqrt{({t_1}^2-1)}}\,dt_1\right\}dz\right] + \frac{2\mu_0 d}{4\pi}\left[\int_{-\frac{W_r}{2}}^{\frac{W_r}{2}} -\frac{d(u_y(z))}{dz}\left\{\int_1^{\infty}\frac{e^{-kt_1\sqrt{(z-z')^2+4(y')^2}}}{\sqrt{({t_1}^2-1)}}\,dt_1\right\}dz\right] \tag{56}$$

$$A_{2z}(z') = \frac{2\mu_0 d}{4\pi}\left[\int_{-\frac{W_r}{2}}^{\frac{W_r}{2}} (-jk)u_y(z)\left\{\int_1^{\infty}\frac{e^{-kt_1(z-z')}}{\sqrt{({t_1}^2-1)}}\,dt_1\right\}dz\right] + \frac{2\mu_0 d}{4\pi}\left[\int_{-\frac{W_r}{2}}^{\frac{W_r}{2}} (-jk)u_y(z)\left\{\int_1^{\infty}\frac{e^{-kt_1\sqrt{(z-z')^2+4(y')^2}}}{\sqrt{({t_1}^2-1)}}\,dt_1\right\}dz\right] \tag{57}$$

The above expressions are again discretized and the following matrix equation can be obtained:

$$[A_{2x}] = [H_1]\left[\frac{du_y}{dz}\right] \tag{58}$$

$$[A_{2z}] = [H_2]\left[u_y\right] \tag{59}$$

where, the elements of matrices $[H_1]$ and $[H_2]$ are known in terms of $\mu_0, d$ and grid point coordinates. The column matrices $[A_{2x}], [A_{2z}]$, $\left[u_y\right]$ and $\left[\frac{du_y}{dz}\right]$ have for their elements, the corresponding values at the grid points.

**Step 4:** Using the central difference method, the matrix $\left[\frac{du_y}{dz}\right]$ can be expressed as:

$$\left[\frac{du_y}{dz}\right] = [S_1]\left[u_y\right] \tag{60}$$

where, $[S_1]$ is the coefficient matrix in terms of the grid coordinates along the z-direction. While forming the matrices, the boundary lines of the rotor sheet along its width are considered as $u_y = 0$ lines for satisfying the conditions in Eq. (40) connected with the differential Eq. (33)

**Step 5:** Substituting for $\left[\frac{du_y}{dz}\right]$ from Eq. (60) in (58), $[A_{2x}]$ can be expressed as:

$$[A_{2x}] = [H_1][S_1]\left[u_y\right] = [M_1]\left[u_y\right] \tag{61}$$

where, $[M_1] = [H_1][S_1]$

**Step 6:** $B_{y2|_{(x',y',z')}} = \left\{\left.\frac{\partial A_{2x}}{\partial z'}\right|_{(x',y',z')} - \left.\frac{\partial A_{2z}}{\partial x'}\right|_{(x',y',z')}\right\} = e^{-jkx'}\left\{\frac{dA_{2x}(z')}{dz'} + jkA_{2z}(z')\right\}$ (62)

where, $A_{2x}(z')$ and $A_{2z}(z')$ are functions of $z'$ only:

$$\text{Also } B_{y2|_{(x',y',z')}} = \{B_{y2}(z')\}e^{-jkx'} \tag{63}$$

where, $B_{y2}(z')$ is a function of $z'$ only. From Eq. (62) and (63) we can write:

$$B_{y2}(z') = \frac{dA_{2x}(z')}{dz'} + jkA_{2z}(z') \tag{64}$$

After discretizing the expression for $B_{y2}(z')$ in Eq. (64), we obtain a matrix equation:

$$\left[B_{y2}\right] = \left[\frac{dA_{2x}}{dz'}\right] + jk[A_{2z}] \tag{65}$$

**Step 7:** Using the forward difference method we can write:

$$\left[\frac{dA_{2x}}{dz'}\right] = [S_2][A_{2x}] \tag{66}$$

where, $[S_2]$ is a known coefficient matrix. Substituting for $[A_{2x}]$ from Eq. (61) in (66), we obtain:

$$\left[\frac{dA_{2x}}{dz'}\right] = [S_2][M_1]\left[u_y\right] = [M_2]\left[u_y\right] \tag{67}$$

where,

$$[M_2] = [S_2][M_1] \tag{68}$$

**Step 8:** Based on Eq. (59), (65) and (67) we obtain the expression for $\left[B_{y2}\right]$ as:

$$\left[B_{y2}\right] = [M_2]\left[u_y\right] + jk[H_2]\left[u_y\right] = [H]\left[u_y\right] \tag{69}$$

where, $[H]$ is the coefficient matrix given by $[M_2] + jk[H_2]$

**Step 9:** With reference to Eq. (33), we can express $B_y(z')$ as a column vector $\left[B_y\right]$ where:

$$\left[B_y\right] = \left[B_{y1}\right] + \left[B_{y2}\right] \tag{70}$$

Discretizing the L.H.S of Eq. (33) matrix:

$$\left[\frac{d^2u_y}{dz'^2} - k^2u_y\right] = [\text{LAPLACIAN}]\left[u_y\right] \tag{71}$$

where, the coefficient matrix [LAPLACIAN] is expressed in terms of the discretized forms of the second order differential operators. From Eq. (64), (70) and (71) we have:

$$[\text{LAPLACIAN}][u_y] = j\sigma s\omega_s \left[[B_{y1}] + [B_{y2}]\right] \quad (72)$$

**Step 10:** Substituting for $[B_{y2}]$ from Eq. (69) in (72), we obtain:

$$[[\text{LAPLACIAN}] - \text{j}\sigma s\omega_s[H]][u_y] = j\sigma s\omega_s[B_{y1}]$$

$$[u_y] = [[\text{LAPLACIAN}] - \text{j}\sigma s\omega_s[H]]^{-1} j\sigma s\omega_s[B_{y1}] \quad (73)$$

From $[u_y]$ we can find $[B_{y2}]$ using Eq. (69)

**Step 11:** Calculation of $B_x$ and $B_z$ components, the longitudinal and lateral components of flux density in the rotor sheet due to both rotor and stator current are $B_x$ and $B_z$:

$$B_x = B_{x1} + B_{x2}\ ; B_z = B_{z1} + B_{z2} \quad (74)$$

where, $B_{x1}, B_{z1}$ are the components of flux density due to the stator current sheet and $B_{x2}, B_{z2}$ are the components of flux density due to rotor current. As the rotor sheet is of infinite length, $B_{x2}$ and $B_{z2}$ at any field point for a fixed value of $z'$ can be expressed as:

$$B_{x2|_{(x',y',z')}} = B_{x2}(z')e^{-jkx'}; \quad B_{z2|_{(x',y',z')}} = B_{z2}(z')e^{-jkx'} \quad (75)$$

Since $\vec{B} = \nabla \times \vec{A}$, the flux density components will also have a sinusoidal distribution with respect to length. Therefore:

$$B_{x1|_{(x',y',z')}} = B_{x1}(z')e^{-jkx'}; \quad B_{z1|_{(x',y',z')}} = B_{z1}(z')e^{-jkx'} \quad (76)$$

And $B_{z2}(z')$ are functions of $z'$ only. From the relation $\vec{B} = \nabla \times \vec{A}$, we can write:

$$B_{x1} = \frac{\partial A_{1z}}{\partial y'};\ B_{z1} = -\frac{\partial A_{1x}}{\partial y'}\ ;\ B_{x2} = \frac{\partial A_{2z}}{\partial y'};\ B_{z2} = -\frac{\partial A_{2x}}{\partial y'} \quad (77)$$

**Step 12:** If the rotor sheet is placed parallel to the stator surface at a height $y'$ from the later, by the method of central difference $B_{x1}$ and $B_{z1}$ at that height can be calculated as:

$$B_{x1}(i)|_{y'=y'} = \frac{A_{1z}(i)|_{y'=y'+\frac{\Delta y'}{2}} - A_{1z}(i)|_{y'=y'-\frac{\Delta y'}{2}}}{\Delta y'} \quad (78)$$

$$B_{z1}(i)|_{y'=y'} = -\left(\frac{A_{1x}(i)|_{y'=y'+\frac{\Delta y'}{2}} - A_{1x}(i)|_{y'=y'-\frac{\Delta y'}{2}}}{\Delta y'}\right) \quad (79)$$

where, the symbol (i) denotes the (i-th) discretized point in the z-direction. For obtaining the mean values of the flux density components, $B_x$ and $B_z$, in a thin rotor sheet $\Delta y' = d$,where $d$ is the thickness of the rotor sheet.

**Step 13:** For calculation of $B_{x2}(i)$ and $B_{z2}(i)$, we calculate $[u_y]$ for a particular height of rotor sheet above the stator surface. From $[u_y]$, $[A_{2x}]$ and $[A_{2z}]$ are calculated from Eq. (59) and (61). Hence we can express:

$$B_{x2}(i)|_{y'=y'} = \frac{A_{2z}(i)|_{y'=y'+\frac{\Delta y'}{2}} - A_{2z}(i)|_{y'=y'-\frac{\Delta y'}{2}}}{\Delta y'} \quad (80)$$

$$B_{z2}(i)|_{y'=y'} = -\left(\frac{A_{2x}(i)|_{y'=y'+\frac{\Delta y'}{2}} - A_{2x}(i)|_{y'=y'-\frac{\Delta y'}{2}}}{\Delta y'}\right) \quad (81)$$

Again we can take $\Delta y' = d$, where $d$ is the thickness of the rotor sheet. It is to be noted that $B_{x2}$ and $B_{z2}$ have a discontinuity across the rotor sheet. The values calculated above give the average values at the top and bottom surface of the rotor.

**Calculation of forces:** Once the fields and currents in the rotor are known, all the force components are calculated using the established relation $\vec{F} = \vec{J} \times \vec{B}$.

Total time average of propulsion, lateral and levitation forces, $F_{xt}, F_{yt}, F_{zt}$ for unit length of the infinitely long rotor are calculated as:

$$F_{xt} = -\frac{(d\times\Delta z)}{2}\sum_{i=1}^{n} Real\{J_{zr}(i) \times B_y{}^*(i)\} \quad (82)$$

$$F_{zt} = \frac{(d\times\Delta z)}{2}\sum_{i=1}^{n} Real\{J_{xr}(i) \times B_y{}^*(i)\} \quad (83)$$

$$F_{yt} = \frac{(d\times\Delta z)}{2}\sum_{i=1}^{n} Real\{J_{zr}(i) \times B_x{}^*(i) - J_{xr}(i) \times B_z{}^*(i)\} \quad (84)$$

## RESULTS AND DISCUSSION

The above numerical method of solution is applied to predict the various components of flux density and forces for the model under consideration (Chattopadhyay, 1997). The main details of the model are reproduced below:

$W_s = 10.6$ cm; $W_r = 27$ cm; $\omega_s = 314 \frac{\text{rad}}{\text{sec}}$; L = 76 cm; $\sigma$(at 75°C) $= 2.42 \times 10^7 \Omega^{-1}\text{m}^{-1}$; $\tau$ = 28cm; d = 3.08 mm

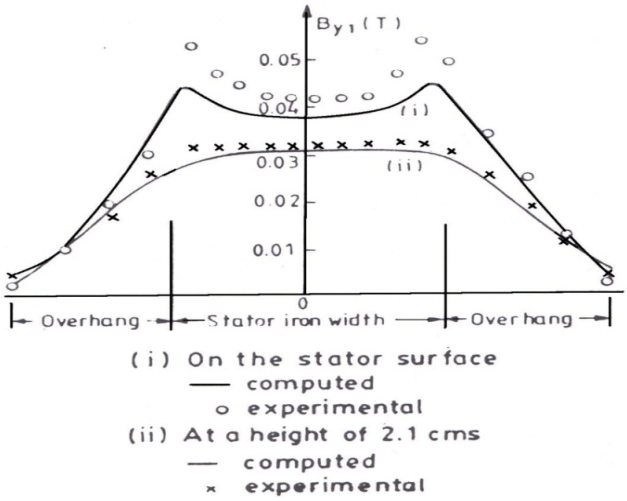


Fig. 3: Flux density (By1) distribution due to stator current (Pucci, 2014)

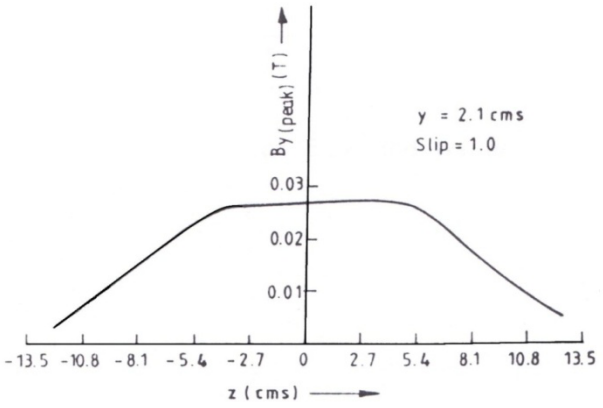


Fig. 4: Distribution of by against z (with rotor)

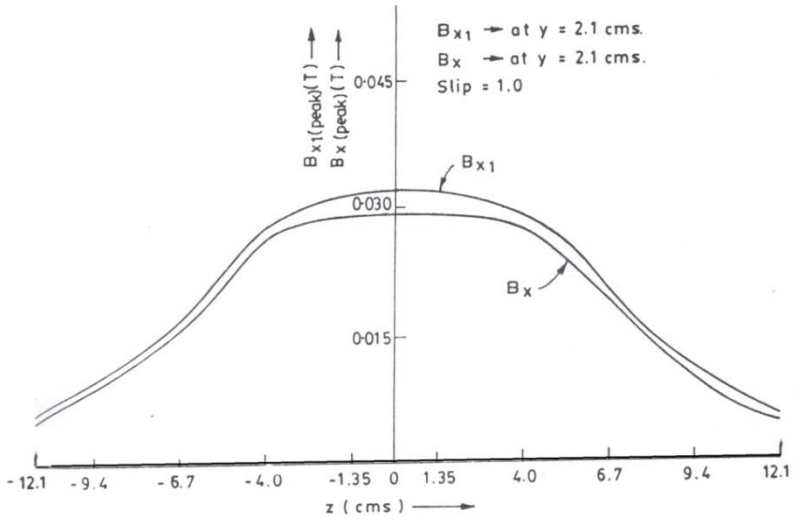


Fig. 5: Variation of Bx1 and Bx against z

Length of stator winding overhang (C) = 8.2 cm; $I_z = 360$ A/cm corresponding to a stator current of 12 A/phase (R.M.S).

**Flux density distribution:** The plots of peak values of $B_{y1}$(due to stator current) based on Eq. (50) to (54) with respect of z, (i) just on the stator surface and (ii) at a

height of 2.1 cm form the stator surface are shown in Fig. 3 for a stator phase current of 12A (R.M.S) which gives a stator linear current density of 360 A/cm. The experimentally found flux density distributions (by using the search coil and mill-voltmeter) are also shown on the same figure. The distributions are quite close to each other.

For the same stator current, the total flux density distribution, $B_y$ on the rotor surface ($y'$ = 2.1 cm) for unity slip is shown in Fig. 4. From this figure, it can be seen that $B_y$ distribution is similar to $B_{y1}$-distribution but has undergone some attenuation due to presence of rotor currents.

Distribution of $B_{x1}$ with 'z' for a stator phase current of 12A (R.M.S) is shown in Fig. 5. In the same figure, the variation of total flux density, $B_x$ (both due to stator and rotor currents) at unity slip is also shown. Once again $B_x$-distribution is similar to $B_{x1}$ distribution but it has undergone some attenuation.

The distribution of $B_{z1}$at a height of 0.725 cm, against z is also shown in Fig. 6. The corresponding measured values are also plotted in the same graph. It can be seen that there is a good correlation between the two values. The total flux density, $B_z$ distribution is once again similar to $B_{z1}$ distribution but very much attenuated due to increased distance from the stator surface and rotor currents.

**Rotor current distribution:** $u_y$ values are calculated at different grid points on the rotor sheet at any chosen slip (say s = 1) for a rotor height of 2.1 cm above the stator surface. The complex values of $u_y$ are multiplied by $e^{j(s\omega_s t - kx)}$ to obtain the instantaneous value, $u_{inst}$ of $u_y$:

$$u_{inst} = Real[u_y(z)e^{j(s\omega_s t - kx)}]$$

By choosing the time instant as zero, $u_{inst}$ values are calculated at different grid points and constant $u_{inst}$ contours are plotted (Fig. 7) over a distance of two pole pitches along the rotor.

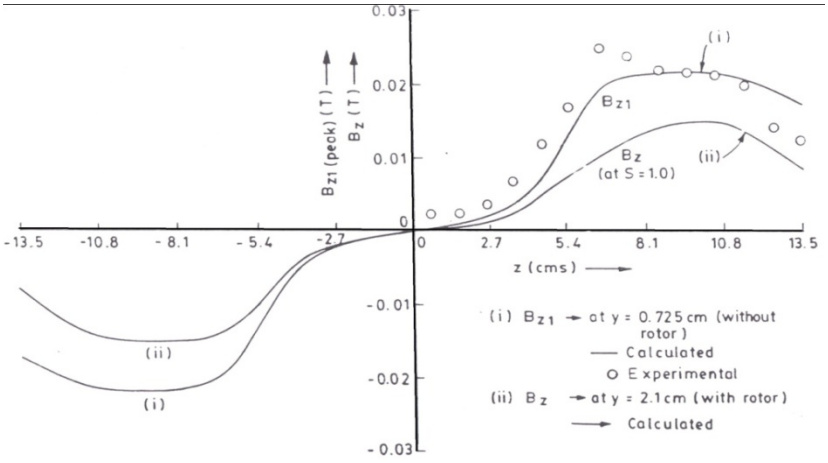


Fig. 6: Distribution of Bz1 against z

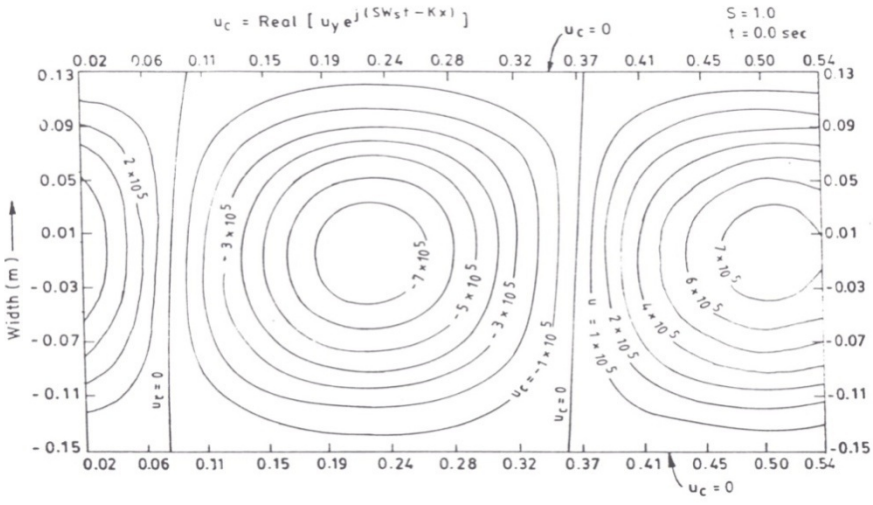


Fig. 7: Typical current distribution in the rotor sheet of infinite length and finite width at a certain instant

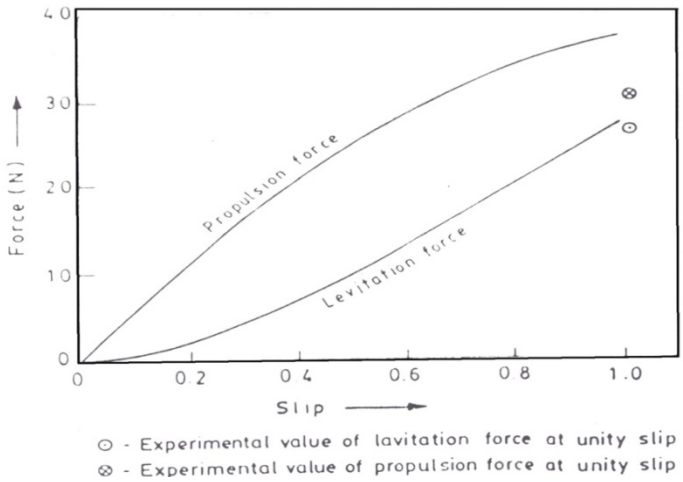


Fig. 8: Variation of propulsion and levitation force with slip based on a rotor model of infinite length and finite width

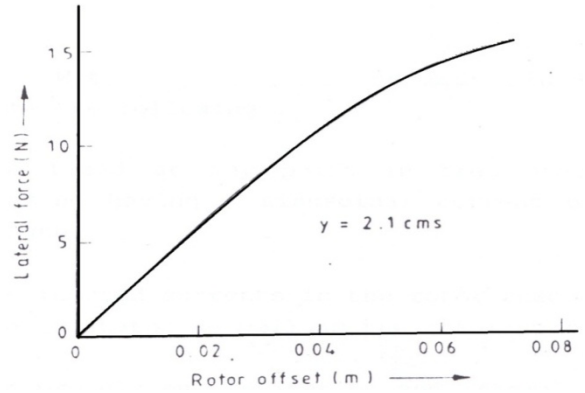


Fig. 9: Variation of lateral force against rotor offset (at unity slip)

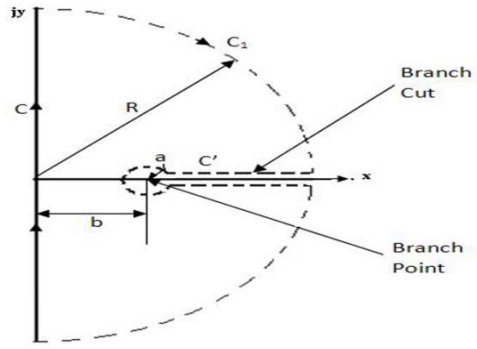


Fig. 10: Path for contour integration

**Forces:** The propulsion and levitation forces per unit length are calculated using Eq. (82) and (84) respectively, for the model under consideration. The above values are multiplied by the actual rotor length (0.76 m) to get the total force on the rotor of the model. By doing so, we are ignoring the discontinuity of the rotor in the longitudinal direction. The forces are calculated for slip varying form s = 0 to s = 1, assuming no rotor offset with respect to the stator width. The simulations are plotted in Fig. 8. The experimental values which could be measured only at s = 1 are also shown in the same figure. Experimental value of levitation force is in good agreement with the calculated value while the experimental value of propulsion force is less than its theoretical value by about 17%. The lateral force per unit length is calculated from Eq. (83) for different rotor offsets in the range 0-7 cm at any chosen value of slip (s = 1). The above values are multiplied by the actual rotor length (0.76 m) to get the total lateral force for the rotor of the experimental model and are plotted in Fig. 9.

## CONCLUSION

In the present study, analysis of a SLIM with a stator and rotor of finite width has been presented. The finite width of the rotor gives rise to peripheral currents in addition to the axial currents which are simultaneously reduced in length. The mathematical formulation and calculation of the fields due to infinitely long but finitely wide stator has been done using special function (Hankel Function) for faster numerical convergence. An integro-differential equation involving the stream function ($u_y$) has been formulated to account for the reaction effect due to the induced currents in the rotor. As the rotor like the stator, is assumed to be infinitely long, the same Hankel function approach has been used for quick solution of $u_y$. Based on $u_y$ values, flux density components due to rotor current have been calculated. Finally the analysis leads to the evaluation of flux density distributions, current contours on the rotor sheet and the propulsion, levitation and lateral forces on the rotor. The observed flux density distributions and the measured forces (at unity slip) in the experimental model have shown reasonable agreement with the corresponding calculated values. The lateral force, which is zero for zero offsets, increases with the rotor

offset indicating that the rotor is inherently unstable in the lateral direction.

Finite Width considerations become a major factor in cases like deciding the weight of the rotor where length and width of the rotor can be compromised. Larger the weight of rotor, more current it will draw from the source, so as to make it stable in the y-direction. Since the source capacity (rating) is limited, development of such model in laboratory becomes crucial, regarding the geometrical dimension factor.

## ACKNOWLEDGMENT

The authors are grateful to the authorities at BITS, Pilani Dubai and IIT Kharagpur for providing the necessary facilities for completing this research work. Also our sincere gratitude is due to Late Dr. Venkataratnam who's valuable and encouraging discussions helped us bring this study in the present shape.

### APPENDIX-1

Evaluation of integral $\int_{-\infty}^{\infty} \frac{e^{-jkx}}{r}\, dx$

Let $p = x - x'$ and $b = \sqrt{(y')^2 + (z - z')^2}$

Hence $\int_{-\infty}^{\infty} \frac{e^{-jkx}}{r}\, dx = e^{-jkx'} \int_{-\infty}^{\infty} \frac{e^{-jkp}}{\sqrt{p^2+b^2}}\, dp$ (85)

Numerical evaluation of integral on right in Eq. (85) is much faster as compared to the integral on left in Eq. (85) For the convenience of notation we replace *p* by *y* so that:

$$\int_{-\infty}^{\infty} \frac{e^{-jkp}}{\sqrt{p^2+b^2}} dp = \int_{-\infty}^{\infty} \frac{e^{-jky}}{\sqrt{y^2+b^2}} dy \quad (86)$$

For ease of evaluating the integral in Eq. (86), it is desirable that the integrand be expressed as a function of $z = x + jy$ so that the contour integration in the complex *z*-plane can be performed. So, we can write:

$$\int_{-\infty}^{\infty} \frac{e^{-jky}}{\sqrt{y^2+b^2}} dy = \int_{z=0-j\infty}^{z=0+j\infty} \frac{e^{-kz}}{\sqrt{z^2-b^2}} dz \quad (87)$$

Where $z = x + jy$ and the path of integration is shown as $c$ in Fig. 10.

The integrand has a branch point singularity at $z = \pm b$. Therefore, a branch cut has been taken along the path $c'$. Paths $c, c_1, c'$ form the closed contour for integration. With reference to Fig. 10, no singularity is trapped in the enclosed portion of the contour as branch cut has been taken along the path $c'$. Therefore summation of the residues of the poles enclosed by the path is zero and hence we can write:

$$\oint_c + \oint_{c_1} + \oint_{c'} = 0 \quad (88)$$

Where the integrand along each path is same and is omitted to avoid repetition. But the integral over $c_1$ is zero, by Jordan's Lemma. So we look at the integral given by:

$$\oint_{c'} \frac{e^{-kz}}{\sqrt{z^2-b^2}} dz = \left(\lim_{a\to 0} 2\int_R^{b+a} \frac{e^{-kx}}{\sqrt{x^2-b^2}} dx\right) + \left(\lim_{a\to 0} 2\int_0^{2\pi} \frac{jae^{-kb}e^{-ak(\cos\theta + j\sin\theta)}e^{j\theta}}{\sqrt{a(2be^{j\theta}+ae^{2j\theta})}} d\theta\right) \quad (89)$$

If $R \to \infty$, the last integral in the R.H.S of Eq. (89) approaches zero because the integrand approaches zero as $a \to 0$.

$$\int_{-\infty}^{\infty} \frac{e^{-jky}}{\sqrt{y^2+b^2}} dy = -\lim_{R\to\infty} \oint_{c'} \frac{e^{-kz}}{\sqrt{z^2-b^2}} dz = 2\int_b^{\infty} \frac{e^{-kb\left(\frac{x}{b}\right)}}{\sqrt{\left(\frac{x}{b}\right)^2 - 1}} d\left(\frac{x}{b}\right) \quad (90)$$

Let $\frac{x}{b} = t_1$, then from the Eq. (90) we get

$$\int_{-\infty}^{\infty} \frac{e^{-jky}}{\sqrt{y^2+b^2}} dy = 2\int_1^{\infty} \frac{e^{-kbt_1}}{\sqrt{t_1^2 - 1}} dt_1 \quad (91)$$

Hence the Eq. (19) is proved in the R.H.S of the Eq. (91).

## REFERENCES

Alonge, F., M. Cirrincione, F. D'Ippolito, M. Pucci and A. Sferlazza, 2014. Parameter identification of linear induction motor model in extended range of operation by means of input-output data. IEEE T. Ind. Appl., 50(2): 959-972.

Boldea, I. and M. Babescu, 1978. Multilayer approach to the analysis of single-sided linear induction motors. P. I. Electr. Eng., 125(4): 283-287.

Chattopadhyay, A.B., 1997. Some experimental and theoretical investigations on the propulsion, levitation and lateral guidance forces in a long stator, short rotor, single sided linear induction motor. Ph.D. Thesis, Indian Institute of Technology (IIT) Kharagpur.

Dos Santos, E.B., J.R. Camacho, A.A. De Paula and G.C. Guimaraes, 2001. Efficiency of the Linear Induction Motor (LIM) performance under constant voltage feeding-additional finite elements considerations. Proceeding of the IEEE Porto Power Tech, Vol. 4.

Freeman, E.M. and D.A. Lowther, 1973. Normal force in single-sided linear induction motors. P. I. Electr. Eng., 120(12): 1499-1506.

Ham, S.H., S.G. Lee, K.S. Kim, S.Y. Cho, C.S. Jin and J. Lee, 2009. Study on reduction of transverse edge effect of single-sided linear induction motor for transportation system. Proceeding of the IEEE Electrical Machines and Systems, ISBN: 978-1-4244-5177-7, pp: 1-4.

Han, J., Y. Li, Y. Du, W. Xu and N. Jin, 2008. Dynamic characteristics study of single-sided linear induction motor with finite element method. Proceeding of the IEEE/ASME International Conference on Advanced Intelligent Mechatronics. Xian, ISBN: 978-1-4244-2494-8, pp: 439-444.

Laithwaite, E.R., 1966. Induction Machines for Special Purposes. Newnes, London.

Lipkins, R.S. and T.C. Wang, 1971. Single Sided Linear Induction motor (SLIM): A study of thrust and lateral forces. Report FRA-RT-72-25. Prepared for Office of High Speed Ground Transportation. Federal Railroad Administration, Washington D.C.

McLean, G.W., 1988. Review of recent progress in linear motors. IEE Proc-B, 135(6): 380-416.

Nasar, S.A., 1976. Linear Electric Machines. Wiley, New York.

Preston, T.W. and A.B.J. Reece, 1969. Transverse edge effects in linear induction motors. P. I. Electr. Eng., 116(6): 973-979.

Pucci, M., 2014. State space-vector model of linear induction motors. IEEE T. Ind. Appl., 50(1): 195-207.

Ratnam, K.V. and A.B. Chattopadhyay, 1996. Analysis of electromagnetic forces in a single-sided short rotor linear induction motor. Proceeding of the International Conference on Power Electronics, Drives and Energy Systems for Industrial Growth. New Delhi, 1: 591-597.

Venkataratnam, K. and A.B. Chattopadhyay, 2002. Analysis of electromagnetic forces in a levitated short rotor LIM-Part I: Finite length and finite width effects. IEEE T. Energy Conver., 17(1): 95-101.

Yang, Z., J. Zhao and T.Q. Zheng, 2008. A novel traction and normal forces study for the linear induction motor. Proceeding of the International Conference on Electrical Machines and Systems. Wuhan, pp: 3474-3477.